Research Article Vol. 31, No. 6 / 13 Mar 2023 / *Optics Express* 10732

Optics EXPRESS

High-performance Ge/Si electro-absorption optical modulator up to 85℃ and its highly efficient photodetector operation

JUNICHI FUJIKATA,[1,2,*] MASATAKA NOGUCHI,[1]
RIKU KATAMAWARI,[3] KYOSUKE INABA,[3] HIDEKI ONO,[1,4]
DAISUKE SHIMURA,[1,4] YOSUKE ONAWA,[1,4] HIROKI YAEGASHI,[1,4]
AND YASUHIKO ISHIKAWA[3]

[1] *Photonics Electronics Technology Research Association (PETRA), Tsukuba, Ibaraki 305-8569, Japan*
[2] *Institute of Post-LED Photonics (pLED), Tokushima University, 2-1, Minami-Josanjima, Tokushima 770-8506, Japan*
[3] *Toyohashi University of Technology, Toyohashi, Aichi 441-8580, Japan*
[4] *Oki Electric Industry Co., Ltd., 1-16-8, Chuo, Warabi, Saitama 335-8510, Japan*
[*] *fujikata.junichi@tokushima-u.ac.jp*

Abstract: We studied a high-speed Ge/Si electro-absorption optical modulator (EAM) evanescently coupled with a Si waveguide of a lateral p–n junction for a high-bandwidth optical interconnect over a wide range of temperatures from 25 °C to 85 °C. We demonstrated 56 Gbps high-speed operation at temperatures up to 85 °C. From the photoluminescence spectra, we confirmed that the bandgap energy dependence on temperature is relatively small, which is consistent with the shift in the operation wavelengths with increasing temperature for a Ge/Si EAM. We also demonstrated that the same device operates as a high-speed and high-efficiency Ge photodetector with the Franz-Keldysh (F-K) and avalanche-multiplication effects. These results demonstrate that the Ge/Si stacked structure is promising for both high-performance optical modulators and photodetectors integrated on Si platforms.

1. Introduction

Silicon photonics has recently attracted considerable attention because of its low cost, low power consumption, and high bandwidth for optoelectronic solutions for applications ranging from telecommunications to chip-to-chip interconnects [1–3]. To realize an effective photonic–electronics convergence system, it is very important to integrate a high-speed optical modulator with a Si-based optical circuit over a wide range of temperatures.

Among the various Si optical modulators (Si-MODs) demonstrated so far, Mach–Zehnder Si-MODs based on the free-carrier plasma dispersion effect have been mostly reported for high-speed modulation and broad-wavelength operation [4–11]. However, carrier-depletion Si modulators require a relatively long phase shifter or a high driving voltage because of the weak plasma dispersion effect in Si [12], and they are not favorable for large-scale integration. It has been reported that ring-resonator-type Si-MODs can realize high-speed and low-power operation. However, the operation wavelength must be controlled to an accuracy of less than 1 nm, which makes practical use difficult [13,14].

To achieve a low-power and high-density interconnect system, an optical modulator with a very small capacitance is required. The GeSi electro-absorption optical modulator (EAM) is promising because its electrical capacitance is approximately 10 fF and the device length is dozens of micrometers [15–19]. It has been reported that a Ge layer on a Si substrate has a tensile strain as large as 0.2%, which reduces the direct band-gap energy from 0.80 eV to 0.77 eV [20]. This leads to an L-band operation of EAMs using such a strained Ge layer. Recently, we have

#484380 https://doi.org/10.1364/OE.484380
Journal © 2023 Received 27 Dec 2022; revised 15 Feb 2023; accepted 24 Feb 2023; published 9 Mar 2023

reported that decreasing the Ge width enabled the EAM to operate in the shorter wavelength range of the C-band [21], although the shift in the operation wavelengths with temperature should be concerned because of the change in the direct bandgap energy. The operating wavelengths of a Ge/Si EAM have been reported to shift to longer wavelengths at high temperatures because the direct bandgap energy decreases with temperature [22]. In addition, a demonstration of a GeSi EAM and Ge photodetector (PD) integrated on a Si platform has been reported, which is promising for a high-density and low-power photonics-electronics convergence system [15–24].

In this paper, we study a high-speed Ge/Si EAM evanescently coupled with a Si waveguide of a lateral p–n junction for a high-bandwidth optical interconnect over a wide range of temperatures from 25 °C to 85 °C. We demonstrated C-band wavelength operation and 56 Gbps high-speed operation at high temperatures up to 85 °C. We also demonstrated a high-responsivity and wide-bandwidth Ge PD in the C + L band wavelengths with the same structure as the EAM. The Franz-Keldysh (F-K) and avalanche-multiplication effects realize the high responsivity with a lower V_{dc} compared with a report on a Ge PD of a vertical p-n junction [25].

2. Experiment and results

2.1. Ge/Si EAM

Figure 1(a) shows a schematic cross-section of a Ge/Si EAM on a Si rib waveguide with a lateral pn junction and cross-sectional TEM (transmission electron microscope) images of a Ge/Si EAM for Fig. 1(b) 0.3μm-width, Fig. 1(c) 0.6μm-width, and Fig. 1(d) 1.0μm-width. The Ge/Si EAM consists of an evanescently coupled structure with a Si rib waveguide [21]. The stack Ge/Si layer width was changed from 0.3 μm to 1.0 μm, and the Ge height was about 300 nm.

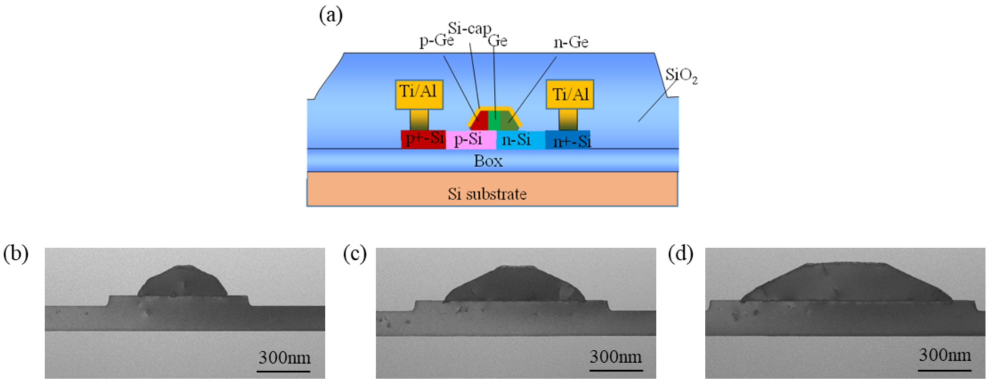

Fig. 1. (a) Schematic diagram of Ge/Si EAM. Cross-sectional TEM image of Ge/Si EAM for (b) 0.3 μm-width, (c) 0.6 μm-width, and (d) 1.0 μm-width.

Figure 2 schematically shows the Ge/Si EAM fabrication process. The fabrication process started from a 300 mm-diameter silicon-on-insulator (SOI) wafer with a 200-nm SOI thickness. Boron (B) and phosphorus (P) ions were implanted into the SOI layer, and the wafers were annealed to form a lateral p–n junction in the SOI layer. Then, a Si pedestal was patterned using immersion ArF lithography and dry etching. Subsequently, nominally 500 nm-thick epitaxial Ge was selectively grown on the Si pedestal using the ultra-high-vacuum chemical vapor deposition method. In the present case, the Ge thickness decreased from 500 nm to approximately 300 nm with a decrease in the Ge width to less than 1 **μ**m because the Ge growth on the (001) crystalline plane is interfered with those on the (111) and (311) sidewall planes. In the Ge epitaxial growth process, we applied a 20-30 nm-thick $Si_{0.5}Ge_{0.5}$ buffer layer, followed by a pure Ge layer growth. After Ge epitaxial growth, a post-annealing process at approximately 800 °C was applied to the wafer for 30 min to improve the crystallinity of the Ge layer on the SOI substrate. Then a 20 nm-thick Si-capping layer was deposited onto the Ge layer to passivate the Ge surface. Next, we implanted B and P ions at the Ge sidewalls with the doping density of $2 \times 10^{18}/\mathrm{cm}^3$ and annealed the wafers to form a lateral p-i-n junction in the Ge layer. Subsequently, a SiO_2 upper-clad layer was deposited, and contact holes were formed by UV lithography and a dry-etching process. Finally, the metal electrodes of the Ti/TiN/Al layers were deposited and patterned.

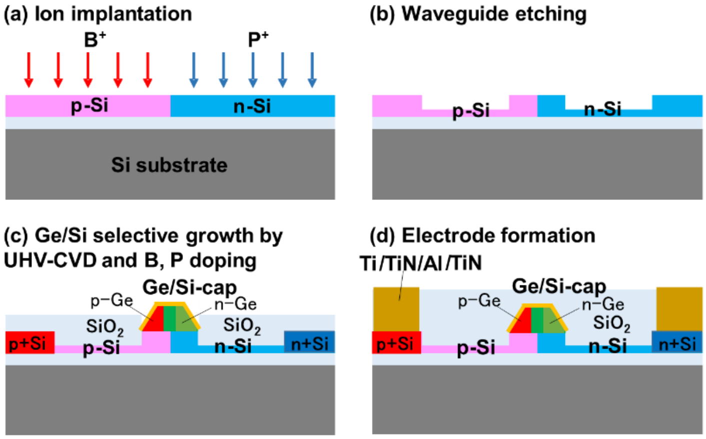

Fig. 2. Fabrication process flow of Ge/Si EAM and Ge/Si PD [21].

Figure 3 shows the frequency EO response for the Ge/Si EAM with 0.3-µm width and 40-µm length at room temperature [21]. Its bandwidth was more than 67 GHz at 2.0 V_{dc}, which is enough for high-speed operation. Figure 4 shows a schematic of the measurement system for the high-speed Ge/Si EAM. A continuous wave (CW) laser light source with a wavelength of 1550 nm and optical power of 13 dBm was applied to the measurement system. Polarization-controlled light was input into the Ge/Si EAM and amplified by an erbium-doped fiber amplifier (EDFA) to detect the optical signal using a sampling oscilloscope or a real-time oscilloscope. To drive the Ge/Si EAM at high speed, an arbitrary waveform generator (AWG) was used to generate high-speed electrical signals of 112 Gbps pulse-amplitude-modulation 4 (PAM-4) and 100 Gbps (non-return-to-zero) NRZ. The high-speed electrical signal to drive the Ge/Si EAM had 1.6 V_{pp} amplitude for the 112 Gbps PAM-4 and 0.8 V_{pp} amplitude for the 100 Gbps NRZ and a V_{dc} of 2.0 V was applied through the bias T. In case of measurement for the high-speed characteristics for the Ge/Si EAM at high temperature, we used the pulse pattern generator (PPG) with 2.5 V_{pp} amplitude for 56 Gbps NRZ and 2.0 V_{dc}.

Figure 5(a) and (b) show the output waveforms of the 112 Gbps PAM-4 and 100 Gbps NRZ with a 2^7-1 psuedo random binary sequence (PRBS) at room temperature. The extinction ratios were 3.1 dB for the 112 Gbps PAM-4 with a 1.6 V_{pp} RF applied voltage and 1.5 dB for the 100 Gbps NRZ with 0.8 V_{pp} RF applied voltage. We demonstrated clear eye opening both for the 112 Gbps PAM-4 and 100 Gbps NRZ modulation formats, which shows that the Ge EAM is promising for high-speed optical interconnects.

Figure 6 shows the experimental results of the optical transmission dependence on the applied voltage at Fig. 6(a) 25 °C, Fig. 6(b) 45 °C, Fig. 6(c) 65 °C, and Fig. 6(d) 85 °C for 0.3-µm-wide and 40-µm-long Ge/Si EAMs. The optical transmission for the Ge/Si EAM is defined as the difference between the optical transmission power of a reference Si channel waveguide and a Si channel waveguide with a Ge/Si EAM in the same chip. It includes the optical coupling loss between a Si WG and Ge/Si EAM. When increasing the reverse bias voltage for a 0.3-µm wide and 40-µm-long Ge/Si EAM at 25 °C, the optical transmission power decreased from -6

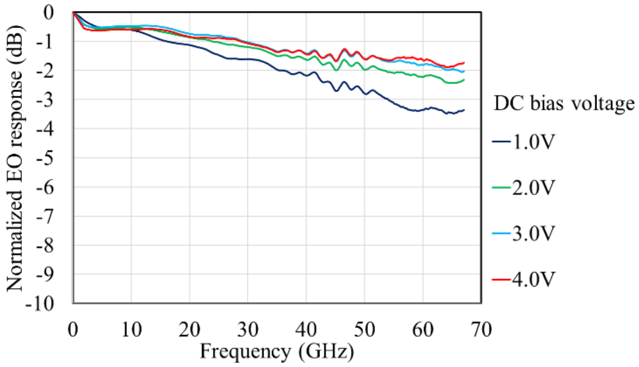

Fig. 3. Frequency EO response for Ge/Si EAM with 0.3-µm width and 40-µm length [21].

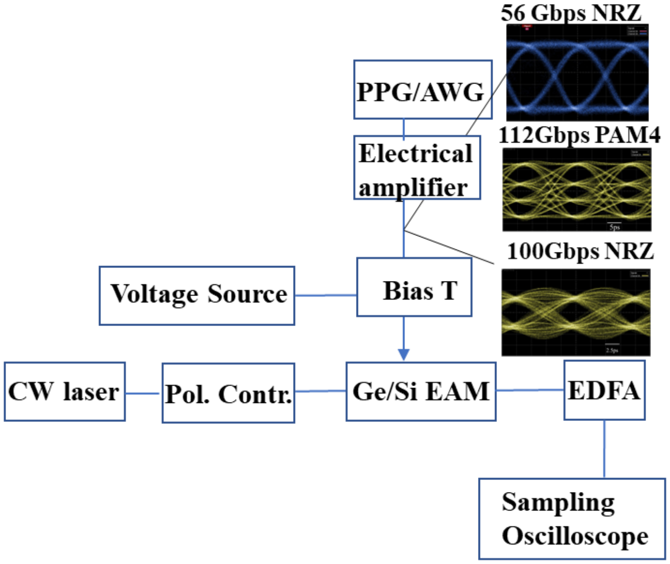

Fig. 4. Schematic diagram of high-speed measurement system for Ge/Si EAM with 0.3-µm width and 40-µm length.

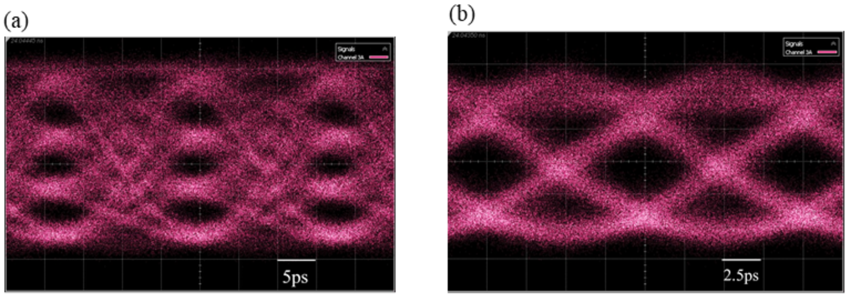

Fig. 5. Output waveforms of (a) 112 Gbps PAM-4 with 2^7-1 PRBS and (b) 100 Gbps NRZ with 2^7-1 PRBS at 1550 nm wavelength, measured at room temperature.

to -9 dB at around a 1550-nm wavelength, which originates from the F-K effect. On the other hand, a 1.0 µm-wide Ge/Si EAM operated at wavelengths between 1580 and 1600 nm, which is consistent with the tensile-strained Ge bandgap energy on Si [19]. The optical transmission spectra for 0.3 µm-wide and 0.6 µm-wide Ge/Si EAMs shifted to shorter wavelengths than that of a 1.0-µm-wide GeSi EAM. This behavior is because the tensile-strain in the smaller-width of a Ge layer is elastically relaxed [26]. From the I-V characteristics, the leakage current of the GeSi EAM is less than 1 µA, which does not affect the optical transmission loss.

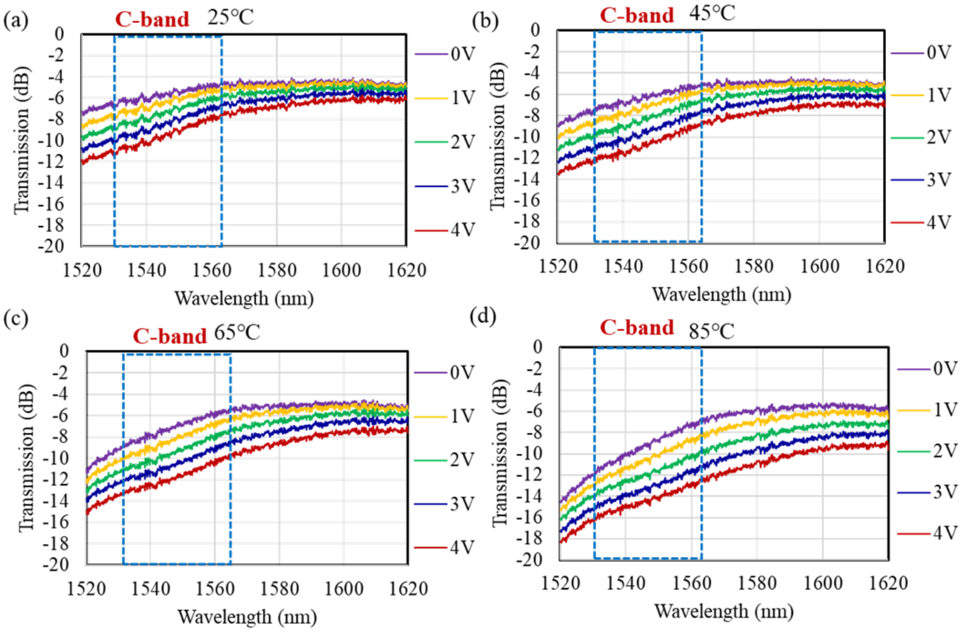

Fig. 6. Experimental results of optical transmission spectrum dependence on V_{dc} for (a) 25°C, (b) 45°C, (c) 65°C, and (d) 85°C.

Figures 7(a) and (b) shows optical transmission spectra at different temperatures and the wavelength at the transmission of -20 dB transmission as a function of temperature, respectively. In this study, absorption edge wavelength was defined as that of optical transmission at -20 dB. With increasing the temperature, the optical absorption edge wavelength shifts to longer wavelength, because direct bandgap energy decreases with temperature [22]. The slope of absorption edge wavelength dependence on temperature was 0.60 nm/°C, which is smaller than that for the previously reported GeSi modulator [16]. Theoretical analysis shows that an increase of Si composition in a GeSi alloy decreases the direct band gap energy and its temperature dependence a little [22]. Therefore, GeSi alloying would affect the temperature dependence of the optical absorption-edge wavelength.

Figure 8 shows photoluminescence (PL) spectrum-peak wavelength dependence on temperature for a bulk Ge layer, a strained Ge layer on Si, and a 0.6 µm-width Ge/Si EAM. In this measurement, an excitation laser wavelength was 785 nm. As for a bulk Ge layer, the slope of PL spectrum peak wavelength vs. temperature was 0.76 nm/°C, which is comparable with the theoretical value [22]. On the other hand, a 0.6 µm-width of Ge/Si EAM shows smaller dependence of PL spectrum peak wavelength on temperature. The slope of the PL spectrum-peak wavelength dependence is 0.54 nm/°C, which is smaller than the theoretical value for $Ge_{0.915}Si_{0.085}$. Therefore, GeSi alloying with various GeSi compositions would contribute to smaller temperature dependence

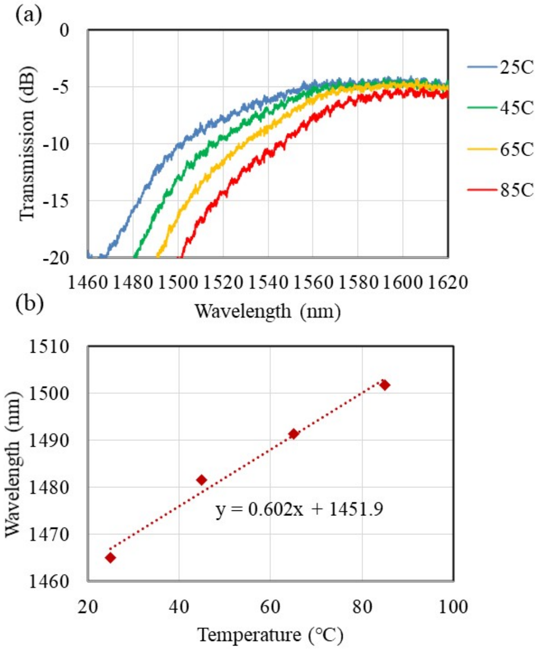

Fig. 7. (a) Experimental result of optical transmission spectrum dependence on temperature and (b) measured wavelength at -20 dB transmission for different temperatures for a GeSi EAM.

of bandgap energy, that is, operation wavelength dependence on temperature for a Ge/Si EAM would decrease with GeSi alloying at the Ge/Si interface.

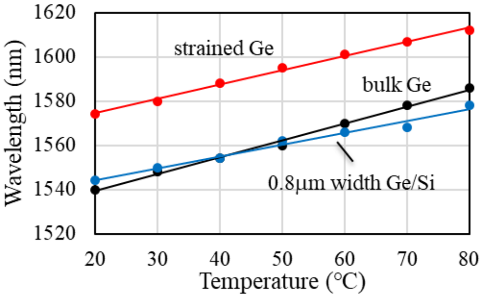

Fig. 8. Photoluminescence-spectrum-peak wavelength dependence on temperature for a bulk Ge layer, a strained Ge layer on Si, and a 0.6 μm-wide Ge/Si EAM.

We analyzed the Ge/Si EAM using Raman spectroscopy with an excitation laser wavelength of 457 nm to investigate the crystalline strain and GeSi alloying of the Ge/Si EAM. From the Raman spectrum, we can verify the GeSi mixed crystalline layer in the Ge/Si stacked structure, in addition to the Ge layer [27,28]. The Raman spectrum peak of Ge-Ge bonding was approximately 298 cm^{-1}, which is consistent with that of a tensile-strained Ge layer. In addition, a small broad peak originating from the GeSi mixed-crystalline structure was observed. Therefore, a GeSi mixed crystalline layer was formed by the Ge epitaxial growth process, which would contribute to the smaller temperature dependence of the operating wavelengths [21,22].

Figure 9(a)–(d) show the output waveforms at 56 Gbps with 2^{31}-1 PRBS (pseudo-random bit sequence) for a 1.55 µm wavelength at 2.0 V_{dc} for a 40 µm-long Ge/Si EAM at 25 °C, 45 °C, 65 °C, and 85 °C. The insertion loss was 5.5 dB, and ER was 3.0 dB at room temperature for the Ge/Si device at 25 °C. In this experiment, optical input power was 3dBm via a lensed optical fiber and optical coupling loss between a lensed optical fiber and the Si waveguide spot size converter was about -2.5 dB. RF drive voltage was 2.5 V_{pp} and V_{dc} was 2.0 V at each temperature. To observe the high-speed output waveform, EDFA was used to maintain the time-averaged output optical power to be -1.2 dBm for each temperature. A clear eye opening was obtained at temperatures up to 85 °C. Extinction ratios were 3.0 dB at 25°C, 3.2 dB at 45°C, 3.0 dB at 60°C, and about 2.0 dB at 85°C. The optical losses at 25°C and 85°C at 1550 nm wavelength were -7 dB and -12 dB at 2.0 V_{dc}. At 85 °C, the optical coupling between a lensed fiber and a Si waveguide for a Ge/Si EAM is unstable in the measurement system, which increases the optical intensity jitter in the output waveform. The frequency bandwidth was greater than 67 GHz for 40 µm length of a Ge/Si EAM. The electrical capacitance was estimated to be approximately 10 fF for the 40 µm length. Therefore, the Ge/Si EAM is promising for low-power and high-bandwidth optical interconnects by improving the insertion optical loss.

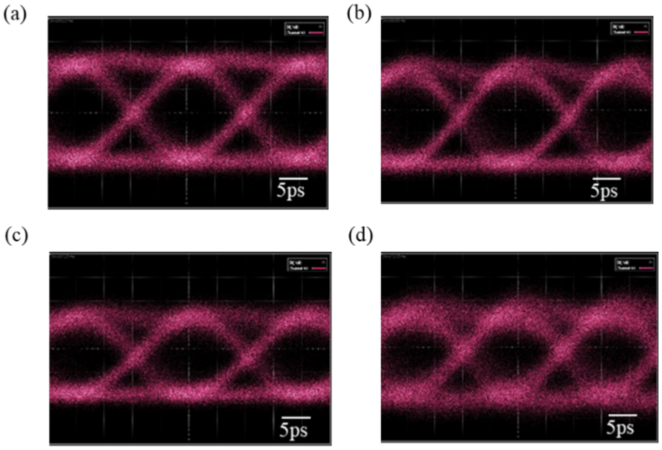

Fig. 9. Output waveforms at 56 Gbps with 2^{31}-1 PRBS for 1.55 µm wavelength at (a) 25°C, (b) 45°C, (c) 65°C, and (d) 85°C for Ge/Si EAM.

3. Ge/Si photodetector

3.1. *High-photoresponsivity by F-K effect*

Next, we studied the photoresponsivity of the Ge–Si stacked structure. Figure 10(a) and (b) show the I-V characteristics and OE response dependence on the frequency and V_{dc} for the 0.3 µm wide and 40 µm-long Ge/Si stacked structure. In this experiment, optical input power was 3dBm via a lensed optical fiber and optical coupling loss between a lensed optical fiber and the Si waveguide spot size converter was about -2.5 dB. With an increase in V_{dc}, the photoresponsivity increased up to approximately 0.83 A/W with 4.0 V_{dc} at 1550 nm wavelength. The 3 dB bandwidth in the OE frequency response was 60 GHz for more than 2 V_{dc}.

Figure 11(a), (b), and (c) show the photoresponsivity dependences on the input light wavelength with increasing V_{dc} for the 0.3 µm, 0.6 µm, and 1.0 µm-wide Ge/Si stacked structures of 40 µm-length. The photoresponsivity enhancement was obtained by the F-K effect with an increase in V_{dc}. As for the 0.3 µm-wide Ge/Si stacked structure, photoresponsivity enhancement by the F-K effect was observed for a large wavelength bandwidth from 1500 nm to 1620 nm. In this

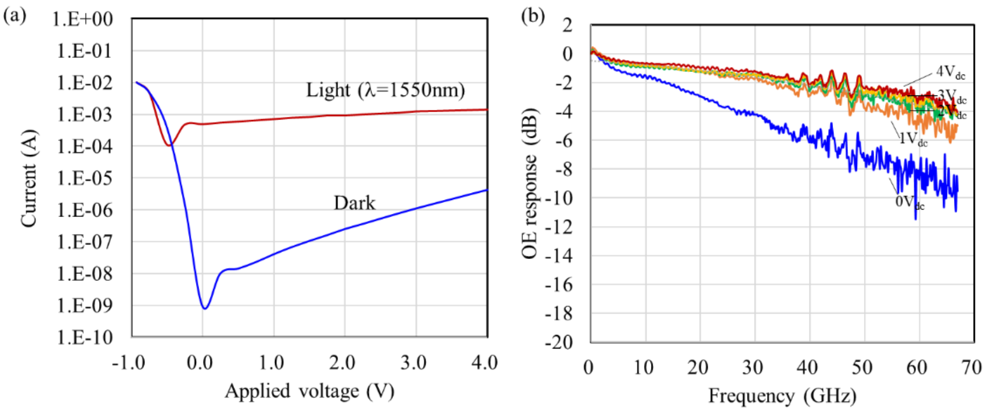

Fig. 10. (a) I-V characteristics with and without 1.55 µm light. (b) Frequency dependence of OE response with 0 to 4 V_{dc}.

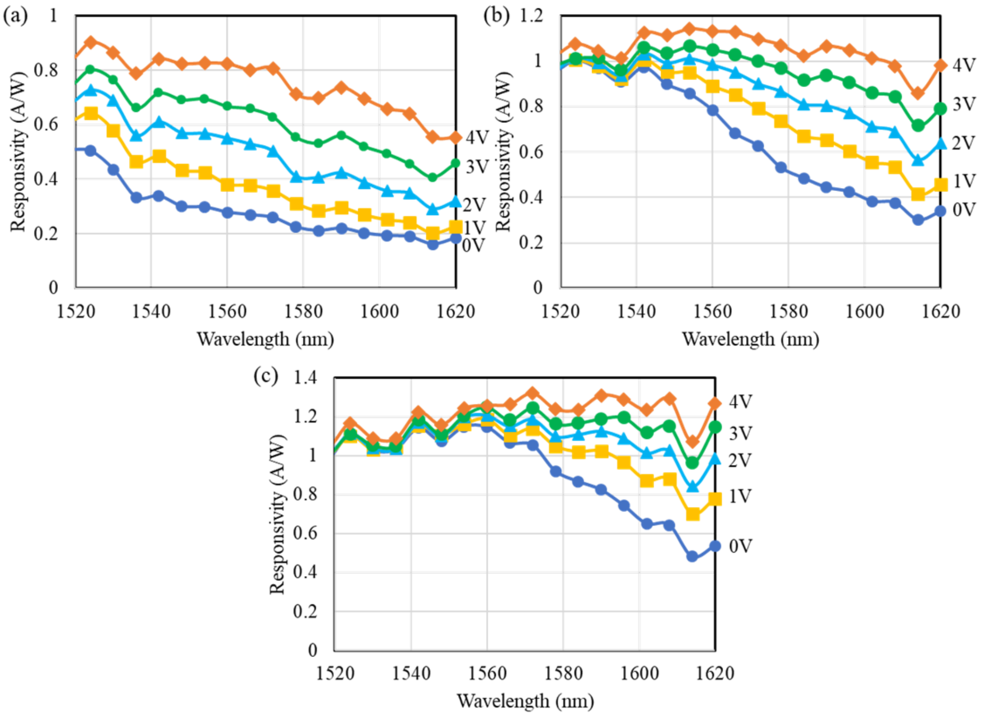

Fig. 11. Bias voltage (V_{dc}) dependence of photoresponsivity for (a) 0.3 µm-width, (b) 0.6 µm-width, and (c) 1.0 µm-width Ge/Si structure of 40 µm-length.

experiment, optical input power was 3dBm via a lensed optical fiber and optical coupling loss between a lensed optical fiber and the Si waveguide spot size converter was measured from 1500 nm to 1620 nm wavelengths. To calculate photoresponsivity, input optical power to the Ge/Si photodetector was calibrated based on the optical coupling loss dependence on wavelength. The wavelength bandwidths with photoresponsivity enhancement by F-K effect shift to longer wavelength for the 0.6 µm and 1.0 µm wide Ge/Si structures. This is because the bandgap in Ge decreases owing to the tensile strain caused by the difference in the thermal expansion coefficients

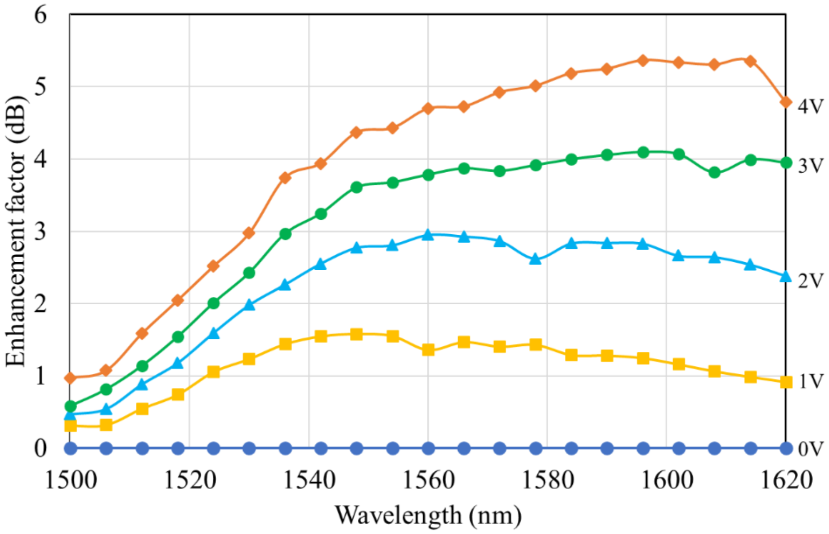

Fig. 12. Photoresponsivity enhancement factor dependence on V_{dc} for 0.3 µm-wide Ge/Si stacked structure of 40 µm-length.

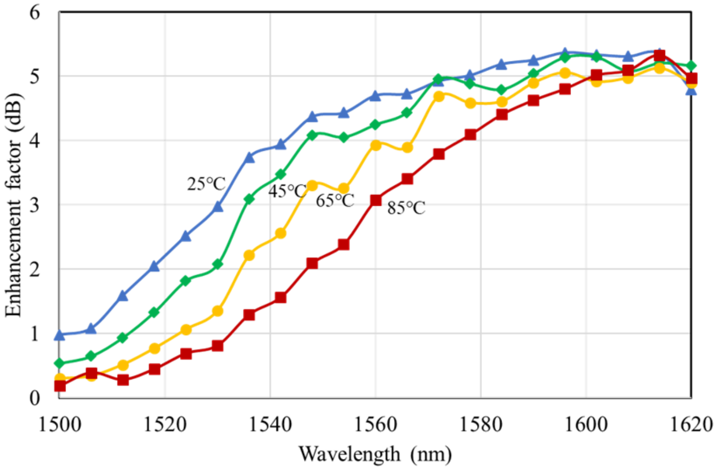

Fig. 13. Photoresponsivity enhancement factor dependence on temperature at $4V_{dc}$ for 0.3 µm-wide Ge/Si stacked structure of 40 µm-length.

of the Ge and Si layers [26]. The smaller width of the Ge/Si stacked structures shows relaxation in tensile strain because of the decrease in the contact area at the Ge/Si stacked interface [26].

Figure 12 shows the enhancement factor of the photoresponsivity dependence on wavelength with an increase in V_{dc} for the 0.3 µm-width Ge/Si stack structure. About 5 dB enhancement of photocurrent could be obtained for larger wavelengths more than 1560 nm. Therefore, the Ge/Si stacked structure with 0.3µm-width shows high-photoresponsivity, high speed, and large bandwidth in the operating wavelengths.

Figure 13 shows the enhancement factor of the photoresponsivity dependence on wavelength with an increase in temperature at 4 V_{dc} for the 0.3 µm-width Ge/Si stack structure. With increase in temperature, optical absorption edge wavelength shift to longer wavelength [29], and photoresponsivity enhancement factor by F-K effect was also observed in the longer wavelength.

Optical absorption edge wavelength dependence on temperature was similar with that shown in Fig. 7(b).

3.2. High-photoresponsivity by the avalanche-multiplication effect

The avalanche-multiplication effect was studied to obtain a higher photoresponsivity in addition to that of the F-K effect [23]. Figure 14(a) and (b) show the I-V characteristics with and without 1.55 µm light and the photoresponsivity dependence on wavelengths with an increase in V_{dc} for a 0.3 µm-wide and 40 µm-long Ge/Si stacked structure. From the I-V characteristics, current amplification by avalanche phenomena in the Ge layer was observed at approximately 5 V_{dc}.

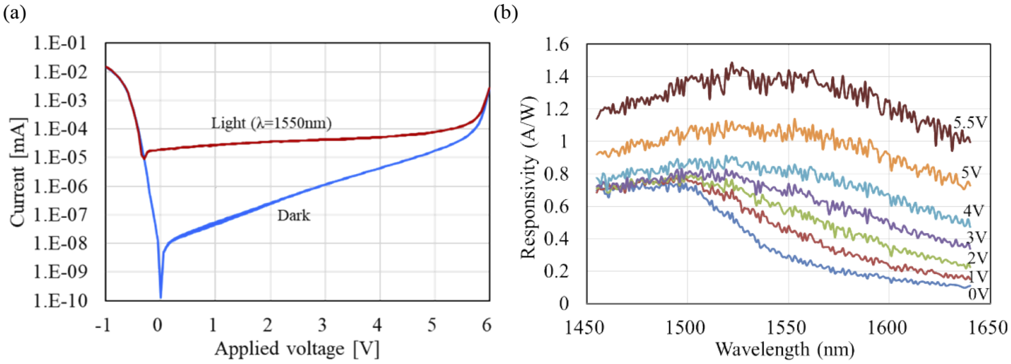

Fig. 14. (a) I-V characteristics with and without 1.55 µm light. (b) Photoresponsivity dependence on wavelengths with increase in V_{dc} for 0.3 µm-wide and 40 µm-long Ge/Si stacked structure.

As shown in Fig. 13(b), the photoresponsivity enhancement by the avalanche effect was measured over a large range of wavelengths greater than 5 V_{dc}. This is different from that of the F-K effect, because the F-K effect is observed mainly around the direct bandgap energy, which is higher than 1500 nm for this device. The multiplication factor of the avalanche multiplication-effect is estimated to be approximately 2. By using the F-K effect and avalanche multiplication-effect, a 7 dB enhancement of photoresponsivity was obtained at a wavelength of 1550 nm.

4. Conclusion

We studied a high-speed Ge/Si EAM evanescently coupled with a Si waveguide of a p–n junction for a high-bandwidth optical interconnect over a wide range of temperatures from 25 °C to 85 °C. We demonstrated 56 Gbps high-speed operation at high temperatures up to 85 °C. From the photoluminescence spectra, we confirmed that the bandgap energy dependence on temperature is relatively small, which is consistent with that of the operation wavelengths with increasing temperature for a Ge/Si EAM. We also demonstrate a high-speed and high-efficiency Ge photodetector. The photoresponsivity was enhanced by the F-K effect and avalanche-multiplication effect in the C + L band wavelengths. These results demonstrate that the Ge/Si stacked structure is promising for both high-performance optical modulators and photodetectors integrated on Si platforms.

Funding. Japan Society for the Promotion of Science (JP21H01367, JP22H01555); New Energy and Industrial Technology Development Organization (JPNP13004).

Acknowledgments. The authors thank the SCR members of AIST for their cooperation in the device fabrication.

Disclosures. The authors declare that there are no conflicts of interest related to this article.

Data availability. Data underlying the results presented in this paper are not publicly available at this time but may be obtained from the authors upon reasonable request.

References

1. G. T. Reed, G. Mashanovich, F. Y. Gardes, and D. J. Thomson, "Silicon optical modulators," Nat. Photonics **4**(8), 518–526 (2010).
2. IEEE 802.3ba 40Gb/s and 100Gb/s Ethernet Task Force, http://www.ieee802.org/3/ba/.
3. InfiniBand Trade Association, http://members.infinibandta.org/kwspub/specs/.
4. W. M. J. Green, M. J. Rooks, L. Sekaric, and Y. A. Vlasof, "Ultra-compact, low RF power, 10 Gb/s silicon Mach-Zhender modulator," Opt. Express **15**(25), 17106–17113 (2007).
5. L. Liao, A. Liu, D. Rubin, J. Basak, Y. Chetrit, H. Nguen, R. Cohen, N. Izhaky, and M. Paniccia, "40 Gbit/s silicon optical modulator for highspeed applications," Electron. Lett. **43**(22), 1196–1197 (2009).
6. F. Y. Gardes, D. J. Thomson, N. G. Emerson, and G. T. Reed, "40 Gb/s silicon photonics modulator for TE and TM polarisations," Opt. Express **19**(12), 11804–11814 (2011).
7. D. J. Thomson, F. Y. Gardes, J. M. Fedeli, S. Zlatanovic, Y. F. Hu, B. P. P. Kuo, E. Myslivets, N. Alic, S. Radic, G. Z. Mashanovich, and G. T. Reed, "50-Gb/s Silicon Optical Modulator," IEEE Photonics Technol. Lett. **24**(4), 234–236 (2012).
8. D. M. Gill, J. E. Proesel, C. Xiong, J. S. Orcutt, J. C. Rosenberg, M. H. Khater, T. Barwics, S. Assefa, S. M. Shank, C. Reinholm, J. Ellis-Monaghan, E. Kiewra, S. Kamlapurkar, C. M. Breslin, W. M. J. Green, W. Haensch, and Y. A. Vlasof, "Demonstration of a High Extinction Ratio Monolithic CMOS Integrated Nanophotonic Transmitter and 16 Gb/s Optical Link," IEEE J. Sel. Topics Quantum Electron. **21**(4), 3400311 (2015).
9. D. Patel, S. Ghosh, M. Chagnon, A. Samani, V. Veerasubramanian, M. Osman, and D. V. Plant, "Design, analysis, and transmission system performance of a 41 GHz silicon photonic modulator," Opt. Express **23**(11), 14263–14287 (2015).
10. M. Liu, X. Yin, E. Ulin-Avila, B. Geng, T. Zentgraf, L. Ju, F. Wang, and X. Zhang, "A graphene-based broadband optical modulator," Nature **474**(7349), 64–67 (2011).
11. Y. Maegami, G. Cong, M. Ohno, M. Okano, K. Itoh, N. Nishiyama, S. Arai, and K. Yamada, "High-efficiency strip-loaded waveguide based silicon Mach-Zhender modulator with vertical p-n junction phase shifter," Opt. Express **25**(25), 31407–31416 (2017).
12. R. Soref and B. R. Bennett, "Electrooptical Effects in Silicon," IEEE J. Quantum Electron. **23**(1), 123–129 (1987).
13. P. Dong, S. Liao, D. Feng, H. Liang, D. Zheng, R. Shafiiha, C.-C. Kung, W. Qian, G. Li, X. Zheng, A. V. Krishnamoorthy, and M. Asghari, "Low V_{pp}, ultralow-energy, compact, high-speed silicon electro-optic modulator," Opt. Express **17**(25), 22484–22490 (2009).
14. G. Li, X. Zheng, J. Yao, H. Thacker, I. Shubin, Y. Luo, K. Raj, J. E. Cunningham, and A. V. Krishnamoorthy, "25Gb/s 1V-driving CMOS ring modulator with integrated thermal tuning," Opt. Express **19**(21), 20435–20443 (2011).
15. J. Liu, M. Beals, A. Pomerene, S. Bernadis, R. Sun, J. Cheng, L. C. Kimerling, and J. Michel, "Waveguide-integrated ultralow-energy GeSi electro-absorption modulators," Nat. Photonics **2**(7), 433–437 (2008).
16. D. Feng, W. Qian, H. Liang, C.-C. Kung, Z. Zhou, Z. Li, J. S. Levy, R. Shafiiha, J. Fong, B. J. Luff, and M. Asghari, "High-Speed GeSi Electroabsorption Modulator on the SOI Waveguide Platform," IEEE J. Sel. Topics Quantum Electron. **19**(6), 3401710 (2013).
17. S. A. Srinivasan, M. Pantouvaki, S. Gupta, H. T. Chen, P. Verheyen, G. Lepage, G. Roelkens, K. Sarawat, D. V. Thourhout, P. Absil, and J. V. Campenhout, "56 Gb/s Germanium Waveguide Electro-Absorption Modulator," J. Lightwave Technol. **34**(2), 419–424 (2016).
18. L. Mastronardi, M. Banakar, A. Z. Khokhar, N. Hattasan, T. Rutirawut, T. D. Bucio, K. M. Grabska, C. Lttlejohns, A. Bazin, G. Mashanovich, and F. Y. Gardes, "High-speed Si/GeSi hetero-structure Electro Absorption Modulator," Opt. Express **26**(6), 6663–6673 (2018).
19. D. A. B. Miller, "Energy consumption in optical modulators for Interconnects," Opt. Express **20**(S2), A293–A308 (2012).
20. Y. Ishikawa, K. Wada, J. Liu, D. D. Cannon, H.-C. Luan, J. Michel, and L. C. Kimerling, "Strain-induced enhancement of near-infrared absorption in Ge epitaxial layers grown on Si substrate," J. Appl. Phys. (Melville, NY, U. S.) **98**(1), 013501 (2005).
21. J. Fujikata, M. Noguchi, K. Kawashita, R. Katamawari, S. Takahashi, M. Nishimura, H. Ono, D. Shimura, H. Takahashi, H. Yaegashi, T. Nakamura, and Y. Ishikawa, "High-speed Ge/Si electro-absorption optical modulator in C-band operation wavelengths," Opt. Express **28**(22), 33123–33134 (2020).
22. L. Wu, Y. Zhou, Y. Cai, X. Cao, R. Wang, M. Qi, J. Fong, D. Feng, and A. Wu, "Design of a broad-band Ge1-xSix electro-absorption based on the Franz-Keldysh effect with thermal tuning," Opt. Express **28**(5), 7585 (2020).
23. A. E. Lim, T. Y. Liow, F. Qing, N. Duan, L. Ding, M. Yu, G. Q. Lo, and D. L. Kwong, "Novel evanescent-coupled germanium electro-absorption modulator featuring monolithic integration with germanium *p-i-n* photodetector," Opt. Express **19**(6), 5040–5046 (2011).
24. Y. Liu, J. Sun, R. Song, X. Li, J. Wang, S. Wang, Y. Yu, W. Yue, Y. Cai, and M. Yu, "80Gb/s NRZ Ge waveguide electro-absorption modulator," Opt. Express **30**(19), 34276–34286 (2022).

25. K. Takeda, T. Hiraki, T. Tsuchizawa, H. Nishi, R. Kou, H. Fukuda, T. Yamamoto, Y. Ishikawa, K. Wada, and K. Yamada, "Contributions of Franz–Keldysh and Avalanche Effects to Responsivity of a Germanium Waveguide Photodiode in the L-Band," IEEE J. Sel. Topics. Quantum. Electron. **20**(4), 3800507 (2014).
26. S. Sonoi, R. Katamawari, M. Shimokawa, K. Inaba, J. A. Piedra-Lorenzana, T. Hizawa, J. Fujikata, and Y. Ishikawa, "Direct Bandgap Control by Narrowing the Germanium Strip Structure on Silicon for C + L Band Photonic Devices," IEEE J. Quantum Electron. **58**(5), 1–9 (2022).
27. S. Nagatomo, Y. Ishikawa, and S. Hoshino, "Near-infrared laser annealing of Ge layers epitaxially grown on Si for high-performance photonic devices," J. Vac. Sci. Technol., B: Nanotechnol. Microelectron.: Mater., Process., Meas., Phenom. **35**(5), 051206 (2017).
28. S. Nagatomo, Y. Kawamata, Y. Izawa, S. Hoshino, and Y. Ishikawa, "Impact of Post-Growth Annealing for Thin-Film Ge Photodiodes on Si," Extended Abst. SSDM2014, 468–469 (2014).
29. Y. P. Varshni, "Temperature dependence of the energy gap in semiconductors," Physica **34**(1), 149–154 (1967).